Stability of the protactinium(V) mono-oxo cation probed by first-principle calculations

Tamara Shaaban, Florent Réal, Rémi Maurice, Valérie Vallet

Stability of the protactinium(V) mono-oxo cation probed by first-principle calculations

Tamara Shaaban,[†] Florent Réal,[†] Rémi Maurice,[‡] and Valérie Vallet[*,†]

[†]*Univ. Lille, CNRS, UMR 8523 - PhLAM - Physique des Lasers Atomes et Molécules, F-59000 Lille, France*

[‡]*Univ Rennes, CNRS, ISCR (Institut des Sciences Chimiques de Rennes) – UMR 6226, F-35000 Rennes, France*

E-mail: valerie.vallet@univ-lille.fr

Abstract

This study explores the distinctive behavior of Protactinium ($Z = 91$) within the actinide series. In contrast to neighboring elements like uranium or plutonium, Protactinium in the pentavalent state diverges by not forming the typical dioxo protactinyl moiety PaO_2^{+} in aqueous phase. Instead, it manifests as a monooxo PaO^{3+} cation or a Pa^{5+}. Employing first-principle calculations with implicit and explicit solvation, we investigate two stoichiometrically equivalent neutral complexes: $PaO(OH)_2(X)(H_2O)$ and $Pa(OH)_4(X)$, where X represents various monodentate and bidentate ligands. Calculating the Gibbs free energy for the reaction $PaO(OH)_2(X)(H_2O) \longrightarrow Pa(OH)_4(X)$, we find that the $PaO(OH)_2(X)(H_2O)$ complex is stabilized with Cl^-, Br^-, I^-, NCS^-, NO_3^-, and SO_4^{2-} ligands, while it is not favored with OH^-, F^-, and $C_2O_4^{2-}$ ligands. Quantum Theory of Atoms in Molecules (QTAIM) and Natural Bond Orbital (NBO) methods reveal the Pa mono-oxo bond as a triple bond, with significant contributions from the 5f and 6d shells. Covalency of the Pa mono-oxo bond increases

with certain ligands, such as Cl^-, Br^-, I^-, NCS^-, and $NO_3{}^-$. These findings elucidate Protactinium's unique chemical attributes and provide insights into the conditions supporting the stability of relevant complexes.

Introduction

Understanding and predicting the physico-chemical properties of radionuclides, in particular actinides, is at the heart of the challenges posed by multiple applications related to environment, energy or health. Questions related to the management of the nuclear fuels used are at the heart of the concerns of our Western societies, and the integrated radioactivity of these nuclei makes them interesting for nuclear medicine. Better understanding of the physical and chemical properties of actinide (An) complexes in the solvated phase, that is to say, their speciation, the nature of the chemical bonds between actinides and their environment partners, their thermodynamic properties, can have direct contributions in societal and industrial applications.

Protactinium ($Z = 91$) stands out as the first actinide element to possess actual 5f electrons in its free-atom ground state ($[Rn]5f^26d^17s^2$). This unique electronic configuration allows for an interplay between the valence 6d and 5f orbitals, making it an intriguing element.[1] However, it also presents challenges in our understanding of its chemistry, as it is one of the most complex and less studied radioactive elements.[2] Protactinium can exist in both the pentavalent and tetravalent oxidation states, similarly to the transition metals niobium and tantalum within the same chemical group. In solution, Pa^V is predominant because Pa^{IV} is unstable and readily oxidizes to Pa^V unless strong reducing conditions are at play.[3]

In this paper, our focus centers on Pa^V. Like its heavier counterparts, uranium, neptunium and plutonium, $PaO_2{}^+$ is stable in the gas phase.[4,5] Both high-level electronic structure calculations and experimental data suggest the monohydrate $PaO_2{}^+(H_2O)$ and the $PaO(OH)_2{}^+$ dihydroxyl complex are isoenergetic.[6–9] However, in solution, the dioxo moiety

PaO_2^+ has not yet been identified.[10–12] Indeed the protactinyl(V) ion is a much stronger acid than its successors in the actinide series and, in fact, the least hydrolyzed species of Pa(V) appears to be $PaO(OH)^{2+}$.[10] Pa^V may exist as a mono-oxo ion PaO^{3+}, in highly acidic media, rendering it a truly unique actinide[12,13] or a sole-cation Pa^{5+}.[14] However, studying Pa^V presents formidable challenges due to its strong tendency towards hydrolysis, polymerization, precipitation and sorption on any solid.[12] To mitigate these competitive reactions, careful control of Pa concentrations and complexing media is essential. Pa^V displays high solubility in hydrofluoric and sulfuric acids, as well as in oxalic acids. Depending on the concentrations and the medium, it can either form oxo complexes or hydroxocomplexes. For instance, Pa^V mono-oxo ion complexes, such as $[PaOF]^{2+}$, $[PaOF_2]^+$, $PaOF_3$, have been postulated in fluoride media under specific hydrofluoric acid concentrations.[15] In concentrated sulfuric acid[16] and oxalic acid,[17] $[PaOL_n]^{3-2n}$ (where L=SO_4^{2-} and $C_2O_4^{2-}$) with stoichiometries ranging from 1:1 to 1:3 have been observed.[11] In cases of higher stoichiometry, X-ray absorption spectroscopy at the PaL_{III} edge has proven useful for confirming the presence or absence of the mono-oxo bond.[13,16–18]

To date, only one crystal structure $[NEt_4]_2[PaOCl_5]$[19] provides evidence of a short Pa-O bond of 1.74 Å. The apparent strength of the Pa−O bond, however, is highly dependent on the concentration and medium, prompting questions about how coordinated ligands and solvent media influence its stability. This issue can be addressed through state-of-the-art quantum calculations. In a study conducted by Toraishi *et al.*, it was concluded that, in the presence of water molecules, Pa^V mono-oxo ionic complexes are the preferable species and that PaO_2^+ does not exist.[20] In our research, we also employ quantum chemical methods to compare the relative stability of the two possible basic units of Pa^V, namely the bare Pa^{5+} and the Pa mono-oxo cation PaO^{3+}. Given that the mono-oxo PaO^{3+} moiety can be regarded as half of an actinyl dioxo cation, it is chemically relevant to discuss the nature of the Pa–O bond in the context of known uranyl complexes for the isoelectronic hexavalent uranium.

Since, Pa^{V} exhibits a closed-shell electronic ground state in most chemical complexes, we will apply single-reference approaches of the density functional theory (DFT) and wave-function Theory (WFT) based approaches, namely the coupled-cluster with single, double and perturbative triple excitations (CCSD(T)), within a relativistic framework. Although relativistic effects, i.e. scalar and spin-orbit ones, are typically considered relevant for open-shell systems, we will also quantify the impact of the spin-orbit coupling on properties of these closed-shell systems, as Vasiliu *et al.*[21] pointed out can amount to about $10\,\mathrm{kJ\,mol^{-1}}$ in Pa^{V} hydrates and hydroxide species.

Choice of Systems

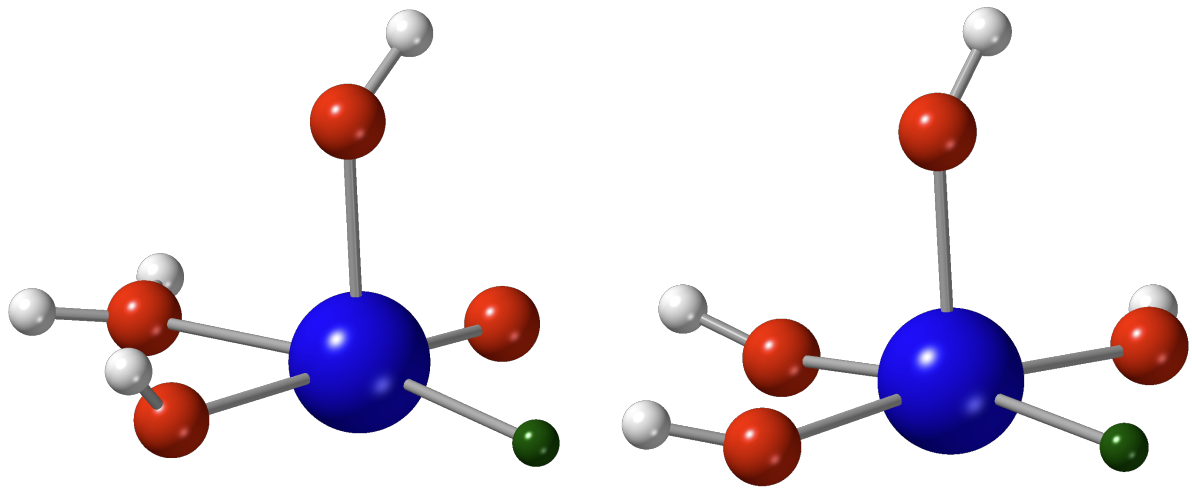

(a) $PaO(OH)_2(F)(H_2O)$ (b) $Pa(OH)_4(F)$

Figure 1: Perspectives of $PaO(OH)_2(F)(H_2O)$ (a) and $Pa(OH)_4(F)$ (b) complexes in water. Color code: navy blue (Pa), dark green (F), red (O), white (H).

Lontchi *et al.*[22] explored the hydrolysis reactions of the dioxo $PaO_2(OH)$ system using relativistic quantum chemical methods. They found that the hydrolysis leads to the exothermic formation of a mono-oxo complex $PaO(OH)_3(H_2O)$ in the first step and $Pa(OH)_5$ in the second step. Their study demonstrated that $Pa(OH)_5$ is more stable by $38.5\,\mathrm{kJ\,mol^{-1}}$ than

the mono-oxo complex $PaO(OH)_3(H_2O)$. This led us to investigate how the substitution of hydroxide OH^- by other ligands influences the stability or instability of the mono-oxo basic form by computing the relative energies of *ad hoc* isomeric complexes. In practice, we chose to expand the study by Lontchi *et al.*[22] by examining two stoichiometrically equivalent neutral complexes $PaO(OH)_2(X)(H_2O)$ and $Pa(OH)_4(X)$, which imply a proton-transfer reaction from the coordinated water molecule to the mono-oxo group in $PaO(OH)_2(X)(H_2O)$. Although these neutral complexes may not be soluble in aqueous solution, our modeling objective is to probe how the X ligands influence their relative stability. In these complexes, the coordination number of Pa^V can vary between 5 and 6 depending on the ligand X. X may be a monodentate or a bidentate ligand. To encompass a wide range of chemical possibilities, we have intentionally selected various ligands, including monodentate ligands , taking as X (X= hydroxide ion OH^-, the halide series F^- (illustrated in Figure 1), Cl^-, Br^-, I^-, with decreasing binding energies with actinide centers,[23] and a monodentate coordinated thiocyanate ligand (NCS^-), as well as bidentate ligands: X = nitrate ($NO_3{}^-$), sulfate ($SO_4{}^{2-}$), that are dominant in natural aquatic systems[10] and the organic oxalate ($C_2O_4{}^{2-}$) ligand. Sulfate and oxalate are known to form complexes with Pa^V.[13,17] The relative complexing tendencies of inorganic anions with respect to Pa^V are:[10]

$$F^- > OH^- > SO_4{}^{2-} > Cl^- > Br^- > I^- > NO_3{}^-. \tag{1}$$

Our primary goal is to provide valuable insights for the experimental community regarding the possible Pa^V complexes that can be formed. To address this question, we will calculate the relative Gibbs free energy corresponding to the reaction:

$$PaO(OH)_2(X)(H_2O)\,[R] \longrightarrow Pa(OH)_4(X)\,[P] \tag{2}$$

Beyond the gas-phase molecular model, we will extend our modeling of $PaO(OH)_2(X)(H_2O)$ and $Pa(OH)_4(X)$ complexes to the bulk phase by considering solvent effects, specifically

water. Solvent effects can be accounted for either implicitly or explicitly. In implicit solvation models, the molecule is enclosed within a cavity surrounded water, which is modeled as a polarizable dielectric continuum. In explicit solvation models, a certain number n of water molecules are included in the first coordination sphere of the complex, and outer hydration shells are modeled by a polarizable continuum model, allowing us to discuss the following reactions for monodentate X ligands:

$$PaO(OH)_2(X)(H_2O)_{(n+1)} \longrightarrow Pa(OH)_4(X)(H_2O)_n \tag{3}$$

where the variable n can take on the value 1, 2 or 3, representing different water coordinations, and making the first-sphere coordination number rise formally from 5 to 8. As discussed later, complexes with three water molecules in the first coordination sphere turned out to be not stable, as one of the water molecules is pushed out to the second coordination sphere, resulting in a maximum coordination number of 7, as found by Oher *et al.*[24]

Computational Details

The geometry optimizations of $PaO(OH)_2(X)(H_2O)_{n+1}$ and $Pa(OH)_4(X)(H_2O)_n$ complexes in their ground state were carried out with ADF.[25,26] These optimizations were performed at the density functional theory (DFT) level employing the B3LYP exchange-correlation functional.[27,28] The solvent effect is taken into account by Conductor-like Screening Model (COSMO).[29–31] All atoms were described using triple-zeta plus polarization (TZ2P) basis sets[32] without freezing core orbitals. To incorporate relativistic effects, two approaches were employed: the scalar relativistic (SR) and spin-orbit (SO) ZORA all-electron Hamiltonians.[33–35] To evaluate the impact of the SOC on the geometries, optimizations were carried out with and without SO for complexes featuring ligands with light atoms (for instance X=OH^-) and a heavier halides (for instance X=I^-). The results, detailed in Table S15 of the Supporting Information, reveal that SO leads to a slight shortening of the Pa-ligand

bond distances, with a maximum reduction of 0.015 Å. This effect is considered negligible, and therefore, structures optimized at the SR level were used. Nevertheless, it is worth noting that the SOC impact on the single-point electronic energies cannot be neglected and was introduced in the calculation of the ΔG_r values by means of a simple correction to the electronic energy ΔE_r, namely ΔE_{SOC}. To ensure that the optimized structures represent minima (no imaginary frequency), harmonic vibration frequency calculations were performed. These calculations also allowed for the determination of the thermodynamics contributions to the Gibbs free energy (ΔG_{corr}).

To calculate the solvation Gibbs free energies (ΔG_{sol}), we have chosen the COSMO-RS[36,37] real-solvent continuum model, using the COSMO-RS atomic radii[38] (Table S1) to construct the continuum model cavities, an approach that is superior to united atom models.[39] COSMO-RS was also found to be superior to other continuum models for the prediction of oxidation potentials.[40] We have validated the COSMO-RS model, by a comparison to other continuum models (PCM and COSMO) for the reaction of interest with X = OH^- and X =$C_2O_4{}^{2-}$, as is discussed and justified in the Supporting Information.

The COSMO-RS solvation model[36,37] as implemented in the COSMOtherm program, utilized files generated by single-point calculations performed with the Gaussian 16 program.[41] In this context the BP86 functional is used, together with def-TZVP basis sets and small core relativistic pseudopotential[42] (60 core electrons) for Pa; and all other atoms were described with def2-TZVP basis sets.[43]

Recognizing that DFT may not provide the ultimate accuracy for determining electronic energies in chemical reactions involving heavy cations,[44–47] additional single-point energy calculations were performed at the CCSD(T)[48] level of theory ($\Delta E_{CCSD(T)}$). CCSD(T) is widely recognized as the reference method in quantum chemistry[49] and is known for its exceptional accuracy, which has motivated the choice of Lontchi *et al.* to explore the Pa^V complexes stability.[22] A discussion of the benchmarking of CCSD(T) versus DFT functionals given in the Supporting Information, supports this assessment.

The CCSD(T) calculations were carried out using the Molpro 2020 software.[50] In the CCSD(T) calculations, relativistic effects were taken into account using all-electron Hamiltonians. Specifically, the choice between the exact two-component relativistic Hamiltonian (X2C)[51] and the Douglas–Kroll–Hess (DKH) Hamiltonian[52] depended in practice on the availability of adequate relativistic atomic basis sets. The aug-cc-pVTZ-X2C basis sets[53–55] were applied for H, O, C, N, S, F, and Cl, while the aug-cc-pVTZ-DK basis sets[56] were utilized for complexes containing Br[57,58] and I.[59] Pa was described appropriately by cc-pVTZ-X2C or cc-pVTZ-DK basis sets.[60] It is worth noting that in CCSD(T) calculations, all valence electrons were correlated, while the core electrons were frozen, except in the case of iodine, for which we had to correlate the outer-core 4d electrons. As it is recognized that CCSD(T) results are sensitive to the quality of the basis sets employed, a basis set quality effects exploration has been operated. Therefore, to attain convergence and determine the most appropriate basis sets, the energy of the reaction 2 with X = OH^- was computed using two different basis sets: VTZ and VQZ. Subsequently, these results were extrapolated to the complete basis set (CBS) limit, which effectively represents an infinitely large basis set (further details are available in the Supplementary Information). The energies obtained for the reaction 2 with X = OH^- using either the VTZ or VQZ basis sets were found to be $-48.3\,\mathrm{kJ\,mol^{-1}}$ and $-48.7\,\mathrm{kJ\,mol^{-1}}$, respectively. When extrapolated to the CBS limit, the reaction energy was determined to be $-48.5\,\mathrm{kJ\,mol^{-1}}$ (See Table S5 of the SI). This convergence study demonstrates that both the VTZ and VQZ basis sets yield reaction electronic energy values very close to the CBS limit. Consequently, it can be concluded that VTZ basis sets are sufficiently accurate for determining the reaction's energy at the CCSD(T) level.

To discuss the relative stabilities of $PaO(OH)_2(X)(H_2O)$ and $Pa(OH)_4(X)$ complexes we calculated the Gibbs free energy ΔG_r of the reaction Equation 2 at room temperature (T=298 K) and at T=319 K and pressure (P=1 bar) summing up the CCSD(T) scalar relativistic energy ($\Delta E_{CCSD(T)}$), the SO correction (ΔE_{SOC}), the thermodynamics correction to the Gibbs free energy (ΔG_{corr}) and the COSMO-RS solvation free energy (ΔG_{sol}) (See

contributions in Table S17 and Table S18 of the SI):

$$\Delta G_r = \Delta E_{CCSD(T)} + \Delta E_{SOC} + \Delta G_{corr} + \Delta G_{sol} \quad (4)$$

The Gibbs free energies reported in Table S16 change by at most 2.4 kJ mol^{-1} when increasing the temperature from 298 K) to T=319 K. Therefore in the rest of the article, only room temperature values will be discussed.

In order to investigate the nature of the chemical bond between Pa and O in the $PaO(OH)_2(X)(H_2O)$ complexes and to assess the extent of involvement of the 5f electrons in chemical bonding, two complementary approaches are employed: natural bond orbital (NBO) analysis and the quantum theory of atoms in molecules (QTAIM), by performing single-point calculations with the B3LYP functional and the COSMO solvent using the ADF software where the NBO6 version[61] is employed. This analysis provides insights into the bonding interactions within molecules, including bond types and electron density distributions. It can reveal the extent to which the 5f and 6d Pa orbitals participate in chemical bonding in the studied complexes. QTAIM provides information about the topology of electron density, such as bond critical points and bond paths. This analysis can help confirm and complement the findings from NBO analysis regarding the nature of chemical bonding in the complexes.

Results and discussion

Solvent effect on geometries with implicit solvation models

The optimization of complex geometries in a solvent like water is essential because it accounts for the influence of the solvent on the molecular structures. In this work, the complexes $PaO(OH)_3(H_2O)$ and $Pa(OH)_5$ (Figure 2) have demonstrated significant structural changes when transitioning from the gas phase to a solvent environment like water. The relaxation effect, quantified by the energy difference between the gas phase and solvent

phase structures, is substantial. In the case of $PaO(OH)_3(H_2O)$, the complex is stabilized by $-76.3\,kJ\,mol^{-1}$ when subjected to geometry optimization in the solvent. Similarly, for $Pa(OH)_5$, it experiences a stabilization of $-28.0\,kJ\,mol^{-1}$ in a solvent environment. This emphasizes the importance of considering solvent effects in studying these complexes, as the solvent can significantly impact their stability and geometry.

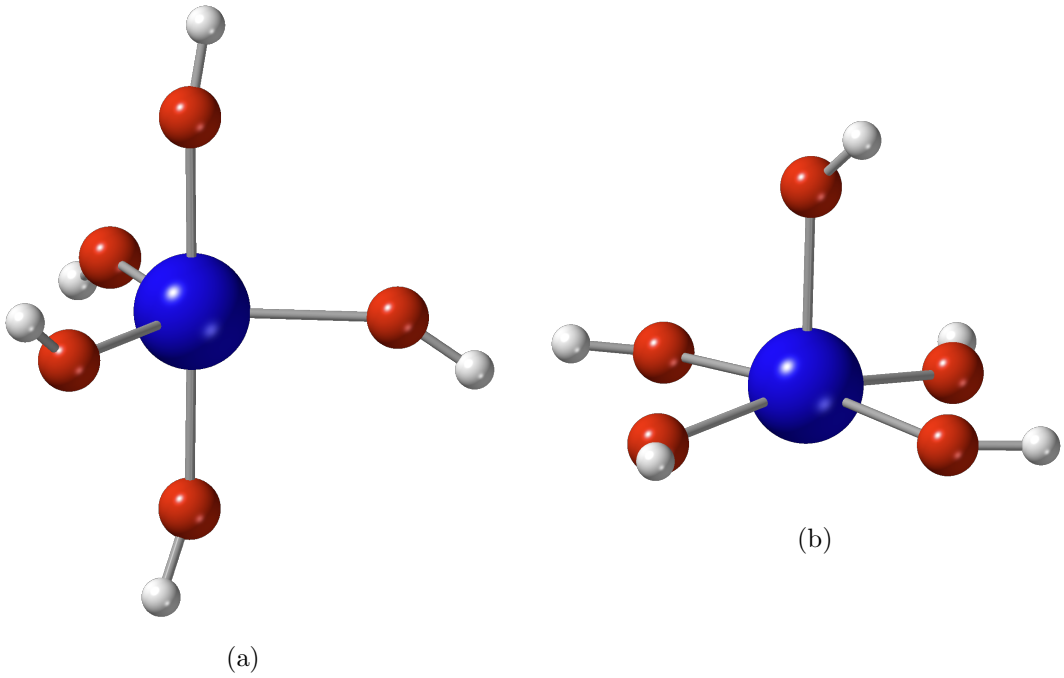

(a) (b)

Figure 2: $Pa(OH)_5$ structures in gas phase (a) and in water (COSMO model) (b). Color code: navy blue (Pa), red (O), white (H).

The comparison of bond lengths between the gas phase and solvent phase structures of $Pa(OH)_4(X)$ and $PaO(OH)_2(X)(H_2O)$ complexes provides valuable insights into the influence of the solvent on these complexes. In the case of $Pa(OH)_4(X)$ complexes, we observe that the Pa–X distance increases by approximately 0.1 Å with various ligands when transitioning from gas phase structures (See Table S6 of the SI) to solvent phase structures (Table 1). Similarly, the Pa–OH distances generally increase by up to 0.1 Å with all ligands, except when using the SO_4^{2-} and $C_2O_4^{2-}$ ligands. This suggests that the solvent environment has a slight elongating effect on these bond distances. However, there does not seem to be a clear trend regarding the Pa–OH distance. On the other hand, for the $PaO(OH)_2(X)(H_2O)$ complexes,

Table 1: Bond distances r (in Å), with their standard deviations within the $Pa(OH)_4(X)$ complexes optimized in the COSMO water solvent at the scalar relativistic level with the B3LYP functional.

X	r(Pa−OH)	r(Pa−X)
OH^-	2.134±0.002	
F^-	2.115±0.010	2.142
Cl^-	2.094±0.006	2.706
Br^-	2.091±0.006	2.876
I^-	2.088±0.019	3.130
NCS^-	2.094±0.006	2.395
NO_3^-	2.094±0.011	2.528±0.007
SO_4^{2-}	2.125±0.013	2.400±0.016
$C_2O_4^{2-}$	2.132±0.008	2.343±0.001

Table 2: Bond distances r (in Å), with their standard deviations and the stretching frequencies ν (in cm^{-1}) of the Pa−O bond within the $PaO(OH)_2(X)(H_2O)$ complexes optimized in the COSMO water solvent at the scalar relativistic level with the B3LYP functional.

X	r(Pa−O)	r(Pa−OH)	r(Pa−X)	r(Pa−OH_2)	ν(Pa−O)
OH^-	1.879	2.164±0.034		2.550	771
F^-	1.871	2.137±0.025	2.181	2.521	779
Cl^-	1.857	2.117±0.028	2.730	2.498	795
Br^-	1.855	2.114±0.028	2.896	2.493	796
I^-	1.852	2.111±0.028	3.140	2.487	799
NCS^-	1.858	2.119±0.026	2.422	2.505	793
NO_3^-	1.860	2.119±0.044	2.547±0.015	2.485	798
SO_4^{2-}	1.873	2.149±0.036	2.440±0.008	2.508	779
$C_2O_4^{2-}$	1.881	2.165±0.040	2.372±0.021	2.525	763

the Pa-O distance increases by a maximum of 0.02 Å, and the Pa-X distance increases by up to 0.1 Å with different ligands when transitioning from gas phase (see Table S7 of the SI) to solvent phase structures (Table 2). Interestingly, the Pa−OH_2 distance decreases by 0.2 Å in water, favoring closer interaction with the central atom Pa.

Overall, these observations emphasize the importance of considering solvent effects when studying these complexes, as they can significantly impact the structural parameters and bonding characteristics of the molecules in a realistic solution environment.

Solvent effect on geometries with explicit solvation models

In the bare $PaO(OH)_2(X)(H_2O)$ and $Pa(OH)_4(X)$ complexes, the coordination number of Pa^V can be either 5 or 6 depending on whether the ligand is monodentate or bidentate. However, it is worth noting that Pa^V can have a coordination number of up to 8.[11,24] This raises the possibility of accommodating additional water molecules in the first coordination sphere of Pa^V in the $PaO(OH)_2(X)(H_2O)$ and $Pa(OH)_4(X)$ complexes. To investigate this hypothesis, we filled the first coordination sphere of $PaO(OH)_2(I)(H_2O)_{n+1}$ and $Pa(OH)_4(I)(H_2O)_n$ complexes with up to $n = 3$ water molecules, as depicted in Figure 3. Our results show that both complexes can accommodate 1 ($n = 1$) and 2 ($n = 2$) additional water molecules. However, when we introduce three water molecules ($n = 3$), the third water molecule migrates to the second coordination sphere, where it forms a hydrogen bond with a first-coordination sphere hydroxide in both complexes, enhancing the overall stability. This suggests that the coordination number of Pa^V is 7 and with monodentate ligands, and could rise up to 8 with bidentate ligands.

To assess the impact of these two additional water molecules on the relative stability of the $PaO(OH)_2(I)(H_2O)_{n+1}$ and $Pa(OH)_4(I)(H_2O)_n$ complexes, we calculated the Gibbs free energies for the reaction $PaO(OH)_2(I)(H_2O)_{(n+1)}$ [R] $\longrightarrow$ $Pa(OH)_4(I)(H_2O)_n$ [P] for n = 0, 1, and 2. Note here that we are looking at difference with respect to the $n = 0$ reaction, computing $\Delta\Delta G_r(n) = \Delta G_r(n) - \Delta G_r(n = 0)$. For n > 0 (Table 3), we observed that first $\Delta\Delta G_r$ are small, and second that the $PaO(OH)_2(I)(H_2O)_{n+1}$ complexes remain more stable than the $Pa(OH)_4(I)(H_2O)_n$ ones, indicating that the addition of up to two water molecules has little impact on the relative stability of the $PaO(OH)_2(I)(H_2O)_{n+1}$ and $Pa(OH)_4(I)(H_2O)_n$ complexes. Given the little impact and that explicit hydration is always tricky, there is no evidence that the corrected $\Delta G_r(n)$ values are there significantly more accurate than the uncorrected one. Therefore, in the remainder of our study, we will focus on discussing the $PaO(OH)_2(X)(H_2O)$ and $Pa(OH)_4(X)$ complexes, without considering explicit hydration.

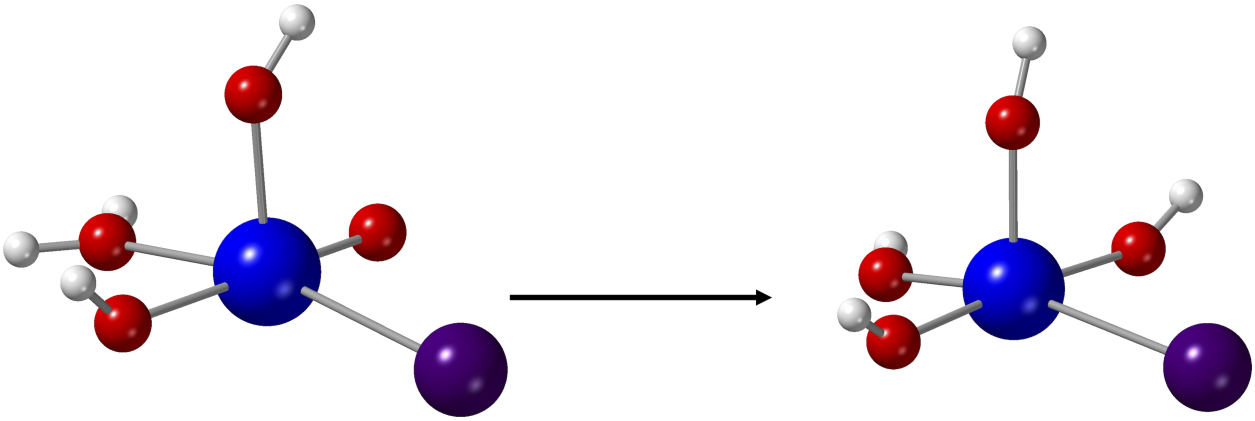

(a) $n = 0$

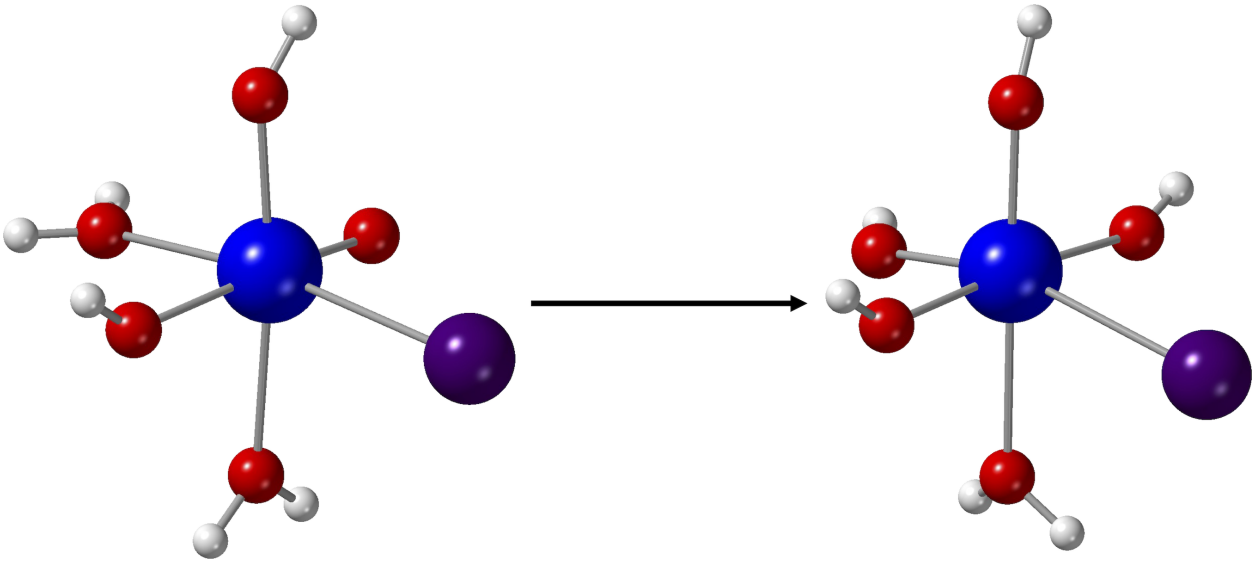

(b) $n = 1$

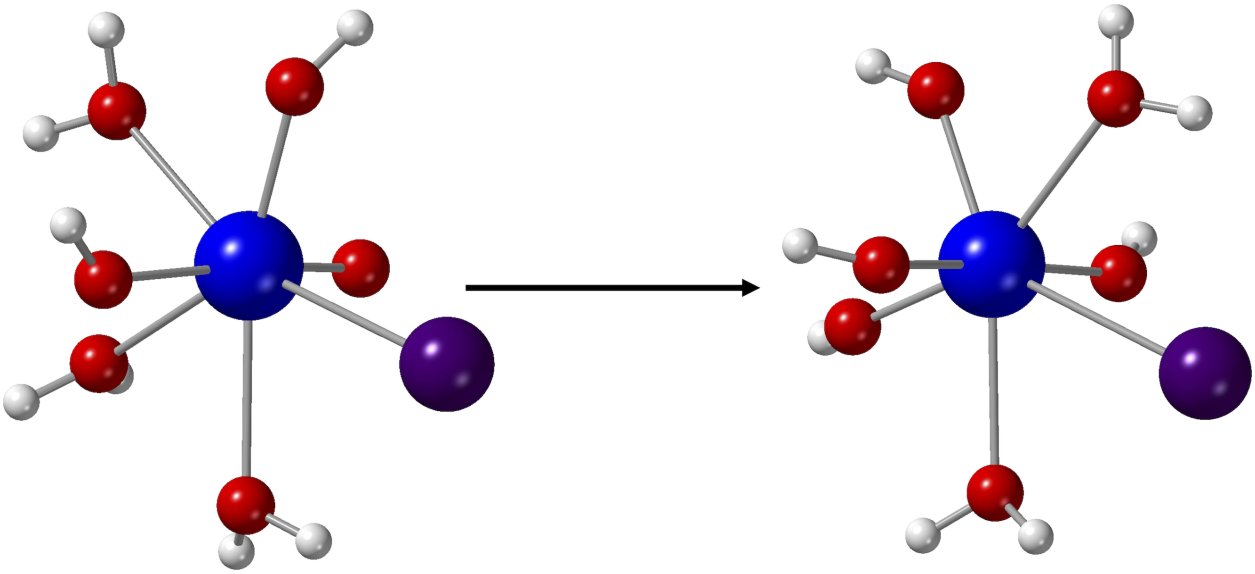

(c) $n = 2$

Table 3: Difference of reaction free energy $\Delta\Delta G_r$ ($\mathrm{kJ\,mol^{-1}}$) of the reaction $PaO(OH)_2(I)(H_2O)_{(n+1)} \longrightarrow Pa(OH)_4(I)(H_2O)_n$ computed at CCSD(T) level, with respect to the reference n=0.

n	1	2	3.0
$\Delta\Delta G_r$-SO	0.2	2.4	3.3

Effect of Spin-Orbit (SO) Coupling on reaction Gibbs free energies

The spin-orbit coupling (SOC) is typically considered to have a negligible effect on the ground-state properties of closed-shell molecular systems such as molecular geometries, which applies to our case. However, since both the compared complexes [P] and [R] display different bonding patterns, it is still possible that the SOC play a secondary but not negligible role on ΔG_r. To test this hypothesis, we calculated the SOC contributions at the scalar relativistic geometries, which in fact amount almost the same order of magnitude to the electronic energies for the reaction $PaO(OH)_2(X)(H_2O) \longrightarrow Pa(OH)_4(X)$ with different ligands, as presented in Table 4. Notably, ΔE_{SO} is negative, in fact remarkably constant $(-5.7\pm0.4)\,\mathrm{kJ\,mol^{-1}}$, indicating that SOC has a more significant stabilizing impact on the Pa complexes compared to the PaO ones. Due to the magnitude of the SOC contribution to ΔG_r, and since we have not found an easy and obvious explanation for this from the 5f and 6d population analysis (see Table S8 of the SI), we just conclude that we cannot disregard the influence of the SOC for the precise determination of the thermodynamics of these reactions.

Effect of ligands (X) on the geometries

The geometries optimized at the DFT/B3LYP level of $Pa(OH)_4(X)$ and $PaO(OH)_2(X)(H_2O)$ complexes are reported in Table 1 and Table 2, respectively. It is noteworthy that in the case of the bidentate ligands NO_3^-, SO_4^{2-}, and $C_2O_4^{2-}$, they form bonds with the Pa^V center through oxygen atoms. When considering NCS^-, there are two possible binding configurations to the Pa^V center, either through the nitrogen atom or through the sulfur

Table 4: Comparison of the electronic reaction energies ΔE_r ($\mathrm{kJ\,mol^{-1}}$) for the reaction $PaO(OH)_2(X)(H_2O) \longrightarrow Pa(OH)_4(X)$ computed at the CCSD(T) level in the gas phase with scalar relativistic effects (SR) and with spin-orbit coupling (SO), with the SO contribution ($\Delta\Delta E_r(SO)$) computed at the B3LYP level in the gas phase.

X	$\Delta E_r(SR)$	$\Delta\Delta E_r(SO)$	$\Delta E_r(SR+SO)$
OH^-	−48.3	−5.3	−53.6
F^-	−37.5	−5.6	−43.1
Cl^-	−27.5	−5.7	−33.2
Br^-	−25.4	−6.1	−31.5
I^-	−25.6	−6.7	−35.5
NCS^-	−24.7	−5.7	−30.4
NO_3^-	−53.4	−5.9	−59.3
SO_4^{2-}	−87.2	−5.2	−92.4
$C_2O_4^{2-}$	−68.6	−5.3	−73.9

atom. Upon optimizing the $Pa(OH)_4(NCS)$ and $Pa(OH)_4(SCN)$ complexes at DFT/B3LYP level, it is observed that $Pa(OH)_4(NCS)$ is energetically more favorable by $33.5\,\mathrm{kJ\,mol^{-1}}$ compared to $Pa(OH)_4(SCN)$. This implies that the Pa^V center prefers to bind to NSC^- through the nitrogen atom rather than the sulfur atom. A similar preference has been reported for An(IV) actinides (An= Th, U and Pu) in a study by Carter *et al.*[62]

For the $PaO(OH)_2(X)(H_2O)$ complexes (See Table 2) and the $Pa(OH)_4(X)$ complexes (See Table 1), a noticeable trend is observed in the variation of the r(Pa−X) distance. The shortest Pa−X distance is found for the OH^- ligand because it is the least bulky ligand. As the halides become heavier (F^-<Cl^-<Br^-<I^-), r(Pa−X) lengthens by up to 0.9 Å compared to the (Pa−F) bond length. Similarly, in the case of bulky ligands such as NO_3^-, SO_4^{2-}, and $C_2O_4^{2-}$, which form bidentate bonds with Pa, the r(Pa−X) is longer by up to 0.4 Å compared to r(Pa−OH). When substituting one hydroxide ligand in the $PaO(OH)_3(H_2O)$ and $Pa(OH)_5$ complexes with X ligands, r(Pa−OH) becomes shorter by at most 0.05 Å in the different $PaO(OH)_2(X)(H_2O)$ and $Pa(OH)_4(X)$ complexes again because OH^- is the least bulky group. The distance to the water molecule, $r(Pa-OH_2)$, remains almost the same among the different $PaO(OH)_2(X)(H_2O)$ complexes. In terms of the r(Pa−O) distance in $PaO(OH)_2(X)(H_2O)$ complexes, it is relevant at this stage to compare the mono-oxo Pa−O

bond distances to the dioxo U−O_{yl} bond distances found in uranyl(VI) complexes with tetra- or pentavalent coordination (Refer to values from the literature listed in Table S9 of the SI). In both the Pa and uranyl complexes, the shorter the An−X distance, the longer the An−O one. We will further discuss the relationship between the coordinated ligand and the Pa−O in the context of its energetic stability. In the literature, experimental values for r(Pa−O) are reported as shorter, such as 1.75 Å in the $PaO(C_2O_4)_3^{3-}$ complex.[16] On the other hand, using the DFT/PBE0 approach,[24] it is 1.86 Å, falling within the same range as r(Pa−O) distances we have reported for the $PaO(OH)_2(X)(H_2O)$ complexes. The origin of this experimental/computational discrepancy is still unclear and requires further investigations both experimentally and computationally, as already mentioned elsewhere.[24]

Pa-ligand bonding analyses

NBO analysis

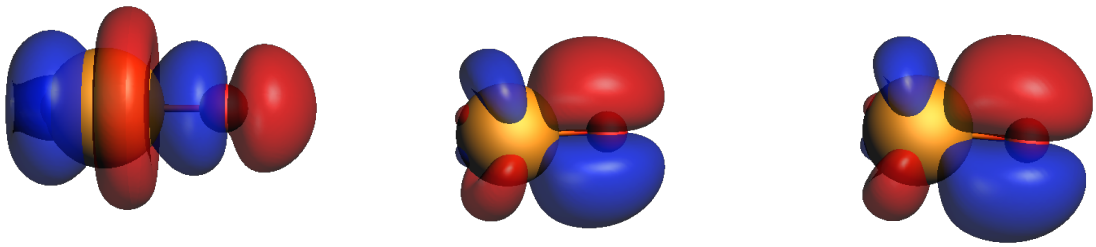

(a) σ orbital (b) π_x orbital (c) π_y orbital

Figure 4: Plots of the σ (a) and two $\pi_{x,y}$ ((b) and (c)) PaO bonding orbitals within the bare PaO^{3+} cation. Color code: yellow (Pa), red (O). The isosurface cutoff is 0.03.

In uranyl (UO_2^{2+}), both U–O formal bond orders are three.[63] In the PaO^{3+} cation, the NBO analysis also reveals a triple bond character (see Figure 4), consisting of one σ bond and two π bonds between Pa and O atoms, all three having occupation numbers nearing 2.

In these σ and π bonding orbitals both the 5f and 6d shells are involved in bonding, with the 5f shell formally receiving more electron from the ligands than the 6d one in both types of orbitals (see Table S10 in the Supporting Information). Note that we consider the Pa^{5+} ion as a reference, and that thus the population of the 5f and 6d shells is conceived as arising from donation from the ligands.

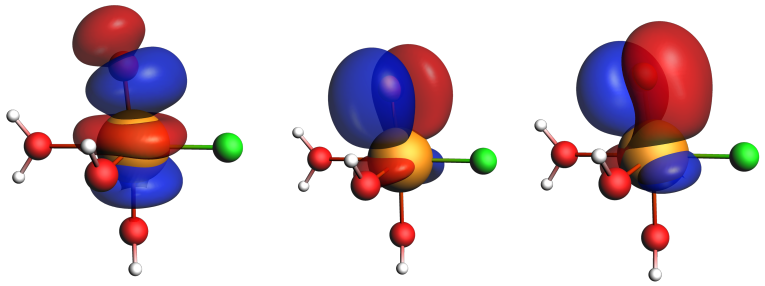

(a) σ orbital (b) π orbital (c) π orbital

Figure 5: Plots of the σ (a) and two π ((b) and (c)) Pa–O bonding orbitals within the $PaO(OH)_2(F)(H_2O)$ complex. Color code: yellow (Pa), green (F), red (O), white (H). The isosurface cutoff is 0.03.

Table 5: Pa (5f and 6d orbitals) and O atomic orbital contributions to the σ and π Pa–O natural localized molecular orbitals (NLMOs) within the $PaO(OH)_2(X)(H_2O)$ complexes.

	σ			π		
X	Pa(5f)	Pa(6d)	O(s/p)	Pa(5f)	Pa(6d)	O(s/p)
OH^-	16.1	5.9	77.3	8.4	7.9	83.5
F^-	16.6	5.7	77.0	8.6	7.9	83.3
Cl^-	17.4	5.6	76.2	8.9	8.2	82.6
Br^-	17.6	5.6	76.1	8.9	8.2	82.6
I^-	17.7	5.6	76.0	8.9	8.2	82.6
NCS^-	16.9	5.9	76.4	9.0	7.9	82.7
NO_3^-	17.3	5.6	76.2	9.1	8.0	82.5
SO_4^{2-}	16.1	5.6	77.5	8.8	8.1	82.8
$C_2O_4^{2-}$	15.7	5.8	77.7	8.5	8.0	83.2

In the $PaO(OH)_2(X)(H_2O)$ complexes, the Pa mono-oxo bond retains its triple bond character as confirmed by the NBO analysis presented in Table 5 and in Figure 5. This analysis reveals that both the σ and two π Pa–O bonds are strongly assymetrical (polarized)

toward the oxygen atom (≈83% oxygen weight), as found in uranyl complexes[64] and that both the 5f and 6d electron contributions from Pa compete in shaping the nature of these bonds. For the σ-bond, the 5f and 6d contributions decrease by approximately by 4 % and 3 %, respectively, when compared to the PaO^{3+} bare cation, implying that the σ bond is more borne by the oxygen atom in the complexes than in the bare PaO^{3+}. In terms of the π bonds, the 5f contribution decreases slightly by 1.9 %, while the 6d contributions marginally increases by 0.6 % in the various $PaO(OH)_2(X)(H_2O)$ complexes compared to PaO^{3+}. Consequently, this makes the 5f and 6d contributions to the π orbitals nearly equivalent in all the studied $PaO(OH)_2(X)(H_2O)$ complexes, and the Pa−O π bonds quite close to the limit of oxygen lone pairs.

QTAIM analysis

To complement the NBO analyses, QTAIM analyses have been performed for the $PaO(OH)_2(X)(H_2O)$ complexes. These analyses provide a range of bonding descriptors defined at the bond critical points (BCPs) which aid in the classification of the nature of the Pa mono-oxo bond, as proposed by Nakainishi *et al.*[65] and Pilmé *et al.*[66] for instance. QTAIM analysis was extensively used to assess the nature of actinide ligand bonds after the pioneering work by Ingram *et al.*[67] In the Supporting Information (see Table S11, Table S12, Table S13, Table S14), we have compiled various bonding BCP descriptors including the electron density (ρ), the Laplacian of the density ($\nabla^2\rho$), kinetic energy density (G), the potential energy density (V), the ratio between the absolute value potential energy density to the kinetic energy one ($|V|$/G), and the charges of the different atoms. The delocalisation index (DI) between two bonded atoms is indicative of the bond order between them. A DI value equal to or lower than 1 suggests a single bond. This criterion applies to the Pa−X, Pa−OH and Pa−OH_2 bonds within the different $PaO(OH)_2(X)(H_2O)$ complexes. In contrast, the DI for the Pa−O bond is approximately 1.8, a value closely resembling that found in uranyl complexes (1.87 to 1.92),[68] where the uranyl bond is recognized as a strongly dissymmetric triple bond. This similarity, in

conjunction with the NBO analysis discussed previously, confirms that the Pa−O bond is a formal triple bond.

In terms of the electron density (ρ), a value of $\rho > 0.2$ a.u. indicates a closed-shell covalent interaction. This criterion applies to the Pa−O bond, while the Pa−X, Pa−OH and Pa−OH_2 bonds within the different $PaO(OH)_2(X)(H_2O)$ complexes are best described as ionic bonds. This classification is further supported by the values of the Laplacian of the density $\nabla^2\rho$ at the BCPs, which are significantly smaller for the Pa−O bond in comparison to the Pa−X, Pa−OH and Pa−OH_2 bonds. Moreover, the ratio between the absolute value potential energy density to the kinetic energy one ($|V|$/G) is a good indicator to describe the chemical bonds. A ratio exceeding 1 suggests a covalent interaction. Significantly, $|V|$/G is higher by 0.5 for the Pa−O bond when compared to that of the Pa−X, Pa−OH and Pa−OH_2 bonds. Thus all QTAIM descriptors collectively support the conclusion that the Pa−O bond exhibits a strong covalent character, while the Pa−X, Pa−OH, and Pa−OH_2 bonds display an ionic character.

Effect of ligands (X) on the relative stabilities of the $PaO(OH)_2(X)(H_2O)$ and $Pa(OH)_4(X)$ complexes

The primary objective of this study was to investigate the influence of inorganic and organic ligands on the relative stability of Pa^{5+} and PaO^{3+} complexes, aiming to identify which ligands can stabilize the Pa^{V} mono-oxo bond stable making it a truly actinide-like.

To determine the relative stability, Gibbs free energies for the reaction $PaO(OH)_2(X)(H_2O) \longrightarrow Pa(OH)_4(X)$ with different X ligands are compared (see Figure 6). A positive ΔG_r translates into a preference for the $PaO(OH)_2(X)(H_2O)$ over the $Pa(OH)_4(X)$ complex. This is the case for Cl^-, Br^-, I^-, NCS^-, $NO_3{}^-$ and $SO_4{}^{2-}$ ligands. Conversely, a negative ΔG_r indicates that the $Pa(OH)_4(X)$ complex is energetically favored over the $PaO(OH)_2(X)(H_2O)$ complex. This is observed with OH^-, F^- and $C_2O_4{}^{2-}$. Note that for thiocyanate ligand, the ΔG_r is close to zero and thus, may be not the most suitable candidate to explore the relative

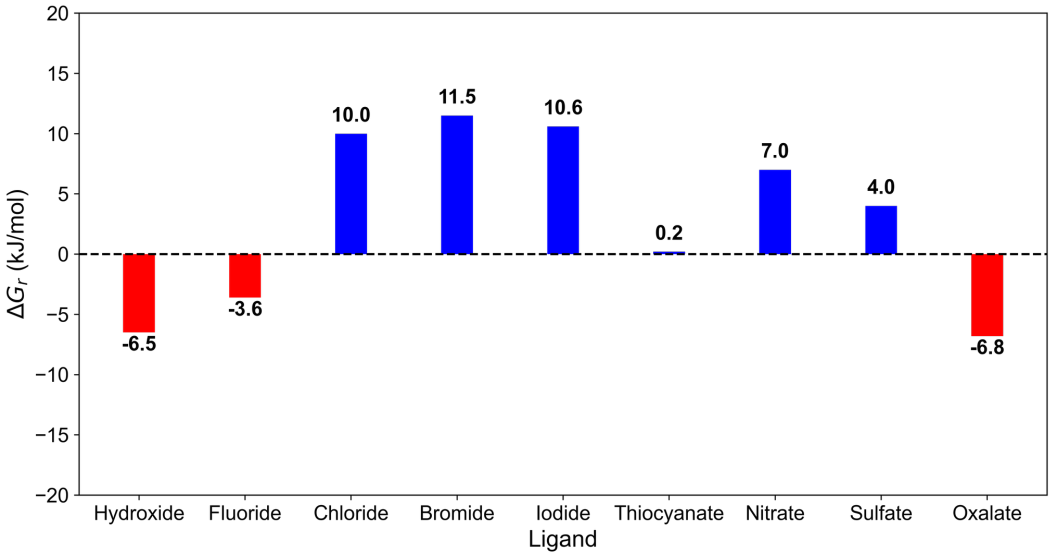

Figure 6: Gibbs free energies (ΔG_r) of the reaction $PaO(OH)_2(X)(H_2O) \longrightarrow Pa(OH)_4(X)$ for the different X ligands in the aqueous phase. The red bars refer to systems in which the X ligand stabilizes $Pa(OH)_4(X)$, and blue bars correspond to $PaO(OH)_2(X)(H_2O)$ being energetically favored.

stability in real conditions. It is noteworthy that the trends in the relative stabilities found in the solvent mirror those in the gas phase (See Figure S1, and Table S17 of the Supporting Information).

The relative stability of these two Pa^V forms can be explained by several factors. One key factor is the length of the Pa–O bond. When the $PaO(OH)_2(X)(H_2O)$ complex is stabilized (as is the case with the Cl^-, Br^-, I^-, NCS^- and NO_3^- ligands), the Pa–O bond is shorter (see Table 2), with a difference of up to 0.03 Å, with respect to the OH^-, F^- and $C_2O_4^{2-}$ ligands. Additionally, the stretching frequency of the Pa–O bond in these complexes is greater by up to 36 cm^{-1} compared to complexes with OH^-, F^- and $C_2O_4^{2-}$ ligands. A shorter Pa–O bond and a higher stretching frequency indicate a stronger Pa–O bond. This phenomenon is observed with Cl^-, Br^-, I^-, NCS^-, and NO_3^- ligands where the $PaO(OH)_2(X)(H_2O)$ complex is stabilized over the $Pa(OH)_4(X)$ complex.

Another crucial factor is the length of the Pa–X bond. The Pa–X bond length is longer by up to 0.9 Å with the Cl^-, Br^-, I^-, NCS^- and NO_3^- ligands compared to the one with

the OH^-, F^-, SO_4^{2-} and $C_2O_4^{2-}$ ligands. Thus, when the $PaO(OH)_2(X)(H_2O)$ complex is stabilized, the Pa^V center exhibits more affinity for the oxygen atom than for the X ligand (X = Cl^-, Br^-, I^-, NCS^- and NO_3^-), leading to the formation a mono-oxo bond. This is not the case of the OH^-, F^- and $C_2O_4^{2-}$ where the $Pa(OH)_4(X)$ complex is stabilized and the Pa–X bond length is shorter indicating stronger bonding between the Pa^V center and these ligands.

In addition, from QTAIM analyses we obtain another important, not fully independent indicator: the DI. It increases as the bond becomes more covalent. This increase in DI is observed when the $PaO(OH)_2(X)(H_2O)$ complex is stabilized over the $Pa(OH)_4(X)$ with Cl^-, Br^-, I^-, NCS^- and NO_3^- ligands (see Table S11 of the Supporting Information). In these cases, the DI is greater by 0.1, compared to the complexes with OH^-, F^- $C_2O_4^{2-}$ ligands.

Concerning the SO_4^{2-} ligand, even if the $PaO(OH)_2(X)(H_2O)$ complex is slightly more stable than the $Pa(OH)_4(X)$ complex, we note that the Pa–O bond distance and the DI deviate from the values obtained for the other ligands Cl^-, Br^-, I^-, NCS^- and NO_3^-, suggesting a weaker Pa–O bond. Thus the SO_4^{2-} ligand may not be a good candidate to observe the Pa mono-oxo bond in experimental conditions.

In summary, a shorter Pa–O bond, a higher stretching frequency, and a larger Pa–O DI all indicate a stronger Pa mono-oxo bond (see Figure 7). This helps explain why the $PaO(OH)_2(X)(H_2O)$ complex is stabilized with Cl^-, Br^-, I^-, NCS^-, and NO_3^- ligands, while the $Pa(OH)_4(X)$ complex is favored with OH^-, F^- and $C_2O_4^{2-}$ ligands.

Conclusion

In our study, our primary objective was to delve into the stability of the Pa–O bond in the presence of various inorganic ligands. Employing advanced quantum chemical methods, we calculated the Gibbs free energy (ΔG_r) for the reaction $PaO(OH)_2(X)(H_2O) \longrightarrow Pa(OH)_4(X)$ under standard conditions. Remarkably, even in closed-shell systems, the in-

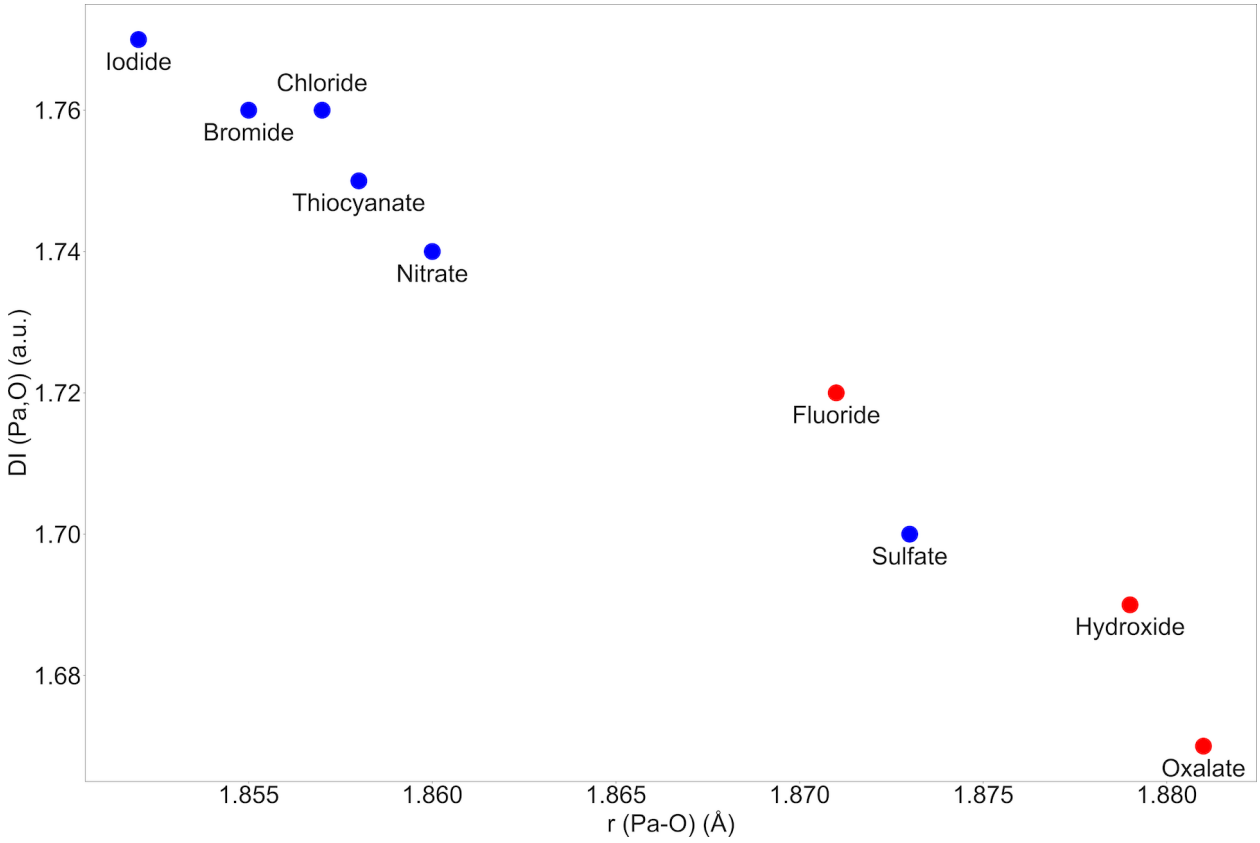

Figure 7: Correlation between the Pa–O bond length (r(Pa–O)) and the delocalisation index of the Pa–O bond (DI(Pa–O)). The red circles refer to systems in which the X ligand stabilizes $Pa(OH)_4(X)$, and blue circles correspond to $PaO(OH)_2(X)(H_2O)$ being energetically favored.

clusion of spin-orbit (SO) coupling significantly impacted the relative electronic energies, and consequently the ΔG_r values. To determine these electronic energies, we utilized the CCSD(T) method, known for its accuracy despite its computational expense. The solvent, water, played a substantial role in structural properties, necessitating geometry optimizations within a water continuum model. Our study introduced additional water molecules to saturate the first coordination sphere, uncovering variations in coordination numbers without affecting the relative stability. The COSMO-RS solvation model was employed for calculating solvation energy (ΔG_{sol}). Additionally, we delved into the nature of the Pa−O bond in both the PaO^{3+} cation and $PaO(OH)_2(X)(H_2O)$ complexes, confirming a triple bond reference (though it is strongly dissymetrical, as the uranyl di-oxo ones).

Predictions regarding the stability of the Pa−O bond indicated preferences for certain ligands, such as the heavier halides (chlorides, bromides, and iodides), as well as nitrates and sulfates. Conversely, hydroxide and oxalate ligands were found to trigger the preferential formation of $Pa(OH)_4(X)$ complexes. We anticipate that these theoretical predictions will serve as a catalyst for future experiments, validating and expanding our understanding of protactinium chemistry.

Acknowledgement

This research received support from the PIA ANR project CaPPA (ANR-11-LABX-0005-01), the ANR CHESS project (ANR-21-CE29-0027), the I-SITE ULNE project OVERSEE (ANR-16-IDEX-0004), the French Ministry of Higher Education and Research, the Hauts de France regional council, and the European Regional Development Fund (ERDF) through projects CPER CLIMIBIO, ECRIN, WaveTech. Additionally, the authors express gratitude for the assistance provided by the French national supercomputing facilities (grants DARI A0130801859, A0110801859). The authors also appreciate the valuable discussions and feedback from ASP. Gomes, M. Maloubier, and C. Le Naour.

Supporting Information Available

All quantum mechanics (QM) data, including the optimized coordinates for all species, are accessible on the open-access Zenodo repository with the following DOI: 10.5281/zenodo.10529027. Version v1.1. Additional results and details are provided in the supporting information PDF file.

References

(1) Wilson, R. Peculiar protactinium. *Nat. Chemistry* **2012**, *4*, 586–586, DOI: 10.1038/nchem.1389.

(2) Myasoedov, B. F.; Kirby, H. W.; Tananaev, I. G. In *The Chemistry of the Actinide and Transactinide Elements*; Morss, L., Edelstein, N., Fuger, J., Eds.; Springer: Dordrecht, 2006; pp 161–252, DOI: 10.1007/1-4020-3598-5_4.

(3) Banik, N. l.; Vallet, V.; Réal, F.; Belmecheri, R. M.; Schimmelpfennig, B.; Rothe, J.; Marsac, R.; Lindqvist-Reis, P.; Walther, C.; Denecke, M. A.; Marquardt, C. M. First structural characterization of Pa(IV) in aqueous solution and quantum chemical investigations of the tetravalent actinides up to Bk(IV): the evidence of a curium break. *Dalton Trans.* **2015**, *45*, 453–457, DOI: 10.1039/C5DT03560K.

(4) Straka, M.; Dyall, K. G.; Pyykkö, P. *Ab initio* study of bonding trends for fˆ0 actinide oxyfluoride species. *Theor. Chem. Acc.* **2001**, *106*, 393–403, DOI: 10.1007/s002140100295.

(5) Gibson, J. K.; Haire, R. G. Gas-Phase Chemistry of Bare and Oxo-Ligated Protactinium Ions: A Contribution to a Systematic Understanding of Actinide Chemistry. *Inorg. Chem.* **2002**, *41*, 5897–5906, DOI: 10.1021/ic025683t.

(6) Dau, P. D.; Wilson, R. E.; Gibson, J. K. Elucidating Protactinium Hydrolysis: The

Relative Stabilities of $PaO_2(H_2O)^+$ and $PaO(OH)_2{}^+$. *Inorg. Chem.* **2015**, *54*, 7474–7480, DOI: 10.1021/acs.inorgchem.5b01078.

(7) Vasiliu, M.; Gibson, J. K.; Peterson, K. A.; Dixon, D. A. Gas Phase Hydrolysis and Oxo-Exchange of Actinide Dioxide Cations: Elucidating Intrinsic Chemistry from Protactinium to Einsteinium. *Chem. Eur. J.* **2019**, *25*, 4245–4254, DOI: 10.1002/chem.201803932.

(8) Jian, T.; Dau, P. D.; Shuh, D. K.; Vasiliu, M.; Dixon, D. A.; Peterson, K. A.; Gibson, J. K. Activation of Water by Pentavalent Actinide Dioxide Cations: Characteristic Curium Revealed by a Reactivity Turn after Americium. *Inorg. Chem.* **2019**, *58*, 14005–14014, DOI: 10.1021/acs.inorgchem.9b01997.

(9) Dau, P. D.; Vasiliu, M.; Wilson, R. E.; Dixon, D. A.; Gibson, J. K. Hydrolysis of Metal Dioxides Differentiates d-block from f-block Elements: Pa(V) as a 6d Transition Metal; Pr(V) as a 4f "Lanthanyl". *J. Phys. Chem. A* **2020**, *124*, 9272–9287, DOI: 10.1021/acs.jpca.0c08171.

(10) Morss, L. R., Edelstein, N. M., Fuger, J., Eds. *The Chemistry of the Actinide and Transactinide Elements*, 4th ed.; Springer: Dordrecht, The Netherlands, 2010; DOI: 10.1007/978-94-007-0211-0.

(11) Le Naour, C.; Roques, J.; Den Auwer, C.; Moisy, P.; Aupiais, J. Protactinium(V) in aqueous solution: a light actinide without actinyl moiety. *Radiochim. Acta* **2019**, *107*, 979–991, DOI: 10.1515/ract-2019-3119.

(12) Le Naour, C.; Maloubier, M.; Aupiais, J. The speciation of protactinium since its discovery: a nightmare or a path of resilience. *Radiochim. Acta* **2022**, *110*, 481–493, DOI: 10.1515/ract-2021-1126.

(13) Di Giandomenico, M. V.; Le Naour, C.; Simoni, E.; Guillaumont, D.; Moisy, P.; Hen-

nig, C.; Conradson, S. D.; Den Auwer, C. Structure of early actinides(V) in acidic solutions. *Radiochim. Acta* **2009**, *97*, 347–353, DOI: 10.1524/ract.2009.1620.

(14) Mendes, M.; Leguay, S.; Le Naour, C.; Hamadi, S.; Roques, J.; Moisy, P.; Guillaumont, D.; Topin, S.; Aupiais, J.; Den Auwer, C.; Hennig, C. Thermodynamic Study of the Complexation of Protactinium(V) with Diethylenetriaminepentaacetic Acid. *Inorg. Chem.* **2013**, *52*, 7497–7507, DOI: 10.1021/ic400378t.

(15) Muxart, R.; Guillaumont, R. *Compléments au nouveau traité de chimie minérale*; masson: Paris, France, 1974; Vol. 2.

(16) Le Naour, C.; Trubert, D.; Di Giandomenico, M. V.; Fillaux, C.; Den Auwer, C.; Moisy, P.; Hennig, C. First Structural Characterization of a Protactinium(V) Single Oxo Bond in Aqueous Media. *Inorg. Chem.* **2005**, *44*, 9542–9546, DOI: 10.1021/ic0512330.

(17) Mendes, M.; Hamadi, S.; Le Naour, C.; Roques, J.; Jeanson, A.; Auwer, C.; Moisy, P.; Topin, S.; Aupiais, J.; Hennig, C.; Di Giandomenico, M.-V. Thermodynamical and Structural Study of Protactinium(V) Oxalate Complexes in Solution. *Inorg. Chem.* **2010**, *49*, 9962–71, DOI: 10.1021/ic101189w.

(18) De Sio, S. M.; Wilson, R. E. EXAFS Study of the Speciation of Protactinium(V) in Aqueous Hydrofluoric Acid Solutions. *Inorg. Chem.* **2014**, *53*, 12643–12649, DOI: 10.1021/ic502376m.

(19) Brown, D.; Reynolds, C. T.; Moseley, P. T. Crystal structure of bis(tetraethylammonium) oxopentachloroprotactinate(V). *J. Chem. Soc., Dalton Trans.* **1972**, 857–859, DOI: 10.1039/DT9720000857.

(20) Toraishi, T.; Tsuneda, T.; Tanaka, S. Theoretical Study on Molecular Property of Protactinium(V) and Uranium(VI) Oxocations: Why Does Protactinium(V) Form Monooxo Cations in Aqueous Solution? *J. Phys. Chem. A* **2006**, *110*, 13303–13309, DOI: 10.1021/jp0641435.

(21) Vasiliu, M.; Peterson, K. A.; Gibson, J. K.; Dixon, D. A. Reliable Potential Energy Surfaces for the Reactions of H_2O with ThO_2, PaO_2^+, UO_2^{2+}, and UO_2. *J. Phys. Chem. A* **2015**, *119*, 11422–11431, DOI: 10.1021/acs.jpca.5b08618.

(22) Lontchi, E. M.; Vasiliu, M.; Tatina, L. M.; Caccamo, A. C.; Gomez, A. N.; Gibson, J. K.; Dixon, D. A. Hydrolysis of Small Oxo/Hydroxo Molecules Containing High Oxidation State Actinides (Th, Pa, U, Np, Pu): A Computational Study. *J. Phys. Chem. A* **2021**, *125*, 6158–6170, DOI: 10.1021/acs.jpca.1c04048.

(23) Grenthe, I.; Gaona, X.; Rao, L.; Plyasunov, A.; Runde, W.; Grambow, B.; Konings, R.; Smith, A.; Moore, E.; Ragoussi, M.-E.; Martinez, J. S.; Costa, D.; Felmy, A.; Spahiu, K. *Second update on the chemical thermodynamics of uranium, neptunium, plutonium, americium and technetium Chemical thermodynamics volume 14*; Nuclear Energy Agency of the OECD (NEA), 2020.

(24) Oher, H.; Delafoulhouze, J.; Renault, E.; Vallet, V.; Maurice, R. Coordination and thermodynamic properties of aqueous protactinium(v) by first-principle calculations. *Phys. Chem. Chem. Phys.* **2023**, *25*, 10033–10041, DOI: 10.1039/D3CP00323J.

(25) te Velde, G.; Bickelhaupt, F. M.; Baerends, E. J.; Fonseca Guerra, C.; van Gisbergen, S. J. A.; Snijders, J. G.; Ziegler, T. Chemistry with ADF. *J. Comput. Chem.* **2001**, *22*, 931–967, DOI: 10.1002/jcc.1056.

(26) ADF2022.103. Place: Vrije Universiteit, Amsterdam, The Netherlands.

(27) Becke, A. D. A new mixing of Hartree–Fock and local density-functional theories. *J. Chem. Phys.* **1993**, *98*, 1372–1377, DOI: 10.1063/1.464304.

(28) Stephens, P. J.; Devlin, F. J.; Chabalowski, C. F.; Frisch, M. J. Ab Initio Calculation of Vibrational Absorption and Circular Dichroism Spectra Using Density Functional Force Fields. *J. Phys. Chem.* **1994**, *98*, 11623–11627, DOI: 10.1021/j100096a001.

(29) Klamt, A.; Schüürmann, G. COSMO: a new approach to dielectric screening in solvents with explicit expressions for the screening energy and its gradient. *J. Chem. Soc., Perkin Trans. 2* **1993**, 799–805, DOI: 10.1039/P29930000799.

(30) Klamt, A. Conductor-like Screening Model for Real Solvents: A New Approach to the Quantitative Calculation of Solvation Phenomena. *J. Phys. Chem.* **1995**, *99*, 2224–2235, DOI: 10.1021/j100007a062.

(31) Klamt, A.; Jonas, V. Treatment of the outlying charge in continuum solvation models. *J. Chem. Phys.* **1996**, *105*, 9972–9981, DOI: 10.1063/1.472829.

(32) Van Lenthe, E.; Baerends, E. J. Optimized Slater-type basis sets for the elements 1–118. *J. Comput. Chem.* **2003**, *24*, 1142–1156, DOI: 10.1002/jcc.10255.

(33) van Lenthe, E.; Baerends, E. J.; Snijders, J. G. Relativistic regular two-component Hamiltonians. *J. Chem. Phys.* **1993**, *99*, 4597–4610, DOI: 10.1063/1.466059.

(34) van Lenthe, E.; Baerends, E. J.; Snijders, J. G. Relativistic total energy using regular approximations. *J. Chem. Phys.* **1994**, *101*, 9783–9792, DOI: 10.1063/1.467943.

(35) van Lenthe, E.; Ehlers, A.; Baerends, E.-J. Geometry optimizations in the zero order regular approximation for relativistic effects. *J. Chem. Phys.* **1999**, *110*, 8943–8953, DOI: 10.1063/1.478813.

(36) Klamt, A.; Eckert, F. COSMO-RS: a novel and efficient method for the a priori prediction of thermophysical data of liquids. *Fluid Phase Equilib.* **2000**, *172*, 43–72, DOI: 10.1016/S0378-3812(00)00357-5.

(37) Klamt, A. The COSMO and COSMO-RS solvation models. *WIREs Comput. Mol. Sci.* **2018**, *8*, e1338, DOI: 10.1002/wcms.1338.

(38) Klamt, A.; Jonas, V.; Bürger, T.; Lohrenz, J. C. W. Refinement and Parametrization of COSMO-RS. *J. Phys. Chem. A* **1998**, *102*, 5074–5085, DOI: 10.1021/jp980017s.

(39) Klamt, A.; Mennucci, B.; Tomasi, J.; Barone, V.; Curutchet, C.; Orozco, M.; Luque, F. J. On the Performance of Continuum Solvation Methods. A Comment on "Universal Approaches to Solvation Modeling". *Acc. Chem. Res.* **2009**, *42*, 489–492, DOI: 10.1021/ar800187p.

(40) Guerard, J. J.; Arey, J. S. Critical Evaluation of Implicit Solvent Models for Predicting Aqueous Oxidation Potentials of Neutral Organic Compounds. *J. Chem. Theory Comput.* **2013**, *9*, 5046–5058, DOI: 10.1021/ct4004433.

(41) Frisch, M. J. et al. Gaussian˜16 Revision C.01. 2016.

(42) Küchle, W.; Dolg, M.; Stoll, H.; Preuss, H. Energy-adjusted pseudopotentials for the actinides. Parameter sets and test calculations for thorium and thorium monoxide. *J. Chem. Phys.* **1994**, *100*, 7535–7542, DOI: 10.1063/1.466847.

(43) Weigend, F.; Ahlrichs, R. Balanced basis sets of split valence, triple zeta valence and quadruple zeta valence quality for H to Rn: Design and assessment of accuracy. *Phys. Chem. Chem. Phys.* **2005**, *7*, 3297–3305, DOI: 10.1039/B508541A.

(44) Gutowski, K. E.; Dixon, D. A. Predicting the Energy of the Water Exchange Reaction and Free Energy of Solvation for the Uranyl Ion in Aqueous Solution. *J. Phys. Chem. A* **2006**, *110*, 8840–8856, DOI: 10.1021/jp061851h.

(45) Wåhlin, P.; Danilo, C.; Vallet, V.; Réal, F.; Flament, J.-P.; Wahlgren, U. An Investigation of the Accuracy of Different DFT Functionals on the Water Exchange Reaction in Hydrated Uranyl(VI) in the Ground State and the First Excited State. *J. Chem. Theory Comput.* **2008**, *4*, 569–577, DOI: 10.1021/ct700062x.

(46) Réal, F.; Trumm, M.; Vallet, V.; Schimmelpfennig, B.; Masella, M.; Flament, J.-P. Quantum Chemical and Molecular Dynamics Study of the Coordination of Th(IV) in Aqueous Solvent. *J. Phys. Chem. B* **2010**, *114*, 15913–15924, DOI: 10.1021/jp108061s.

(47) Kervazo, S.; Réal, F.; Virot, F.; Gomes, A. S. P.; Vallet, V. Accurate Predictions of Volatile Plutonium Thermodynamic Properties. *Inorg. Chem.* **2019**, *58*, 14507–14521, DOI: 10.1021/acs.inorgchem.9b02096.

(48) Purvis, G. D., III; Bartlett, R. J. A full coupled-cluster singles and doubles model: The inclusion of disconnected triples. *J. Chem. Phys.* **1982**, *76*, 1910–1918, DOI: 10.1063/1.443164.

(49) Bartlett, R. J.; Musiał, M. Coupled-cluster theory in quantum chemistry. *Rev. Mod. Phys.* **2007**, *79*, 291–352, DOI: 10.1103/RevModPhys.79.291.

(50) Werner, H.-J. et al. The Molpro quantum chemistry package. *J. Chem. Phys.* **2020**, *152*, 144107, DOI: 10.1063/5.0005081.

(51) Liu, W.; Peng, D. Exact two-component Hamiltonians revisited. *J. Chem. Phys.* **2009**, *131*, 031104, DOI: 10.1063/1.3159445.

(52) Wolf, A.; Reiher, M.; Hess, B. The generalized Douglas-Kroll transformation. *J. Chem. Phys.* **2002**, *117*, 9215–9226, DOI: 10.1063/1.1515314.

(53) Dunning, T. H., Jr. Gaussian basis sets for use in correlated molecular calculations. I. The atoms boron through neon and hydrogen. *J. Chem. Phys.* **1989**, *90*, 1007, DOI: 10.1063/1.456153.

(54) Dunning, T. H., Jr.; Peterson, K. A.; Wilson, A. K. Gaussian basis sets for use in correlated molecular calculations. X. The atoms aluminum through argon revisited. *J. Chem. Phys.* **2001**, *114*, 9244–9253, DOI: 10.1063/1.1367373.

(55) Peterson, K. A. Recontraction for DK. **2018**, unpublished results.

(56) Grant Hill, J.; Peterson, K. A. Gaussian basis sets for use in correlated molecular calculations. XI. Pseudopotential-based and all-electron relativistic basis sets for alkali

metal (K–Fr) and alkaline earth (Ca–Ra) elements. *J. Chem. Phys.* **2017**, *147*, 244106, DOI: 10.1063/1.5010587.

(57) Wilson, A. K.; Woon, D. E.; Peterson, K. A.; Dunning, T. H., Jr. Gaussian basis sets for use in correlated molecular calculations. IX. The atoms gallium through krypton. *J. Chem. Phys.* **1999**, *110*, 7667–7676, DOI: 10.1063/1.478678.

(58) de Jong, W. A.; Harrison, R. J.; Dixon, D. A. Parallel Douglas–Kroll energy and gradients in NWChem: Estimating scalar relativistic effects using Douglas–Kroll contracted basis sets. *J. Chem. Phys.* **2001**, *114*, 48, DOI: 10.1063/1.1329891.

(59) Bross, D. H.; Peterson, K. A. Correlation consistent, Douglas–Kroll–Hess relativistic basis sets for the 5p and 6p elements. *Theor. Chem. Acc.* **2014**, *133*, 1434, DOI: 10.1007/s00214-013-1434-9.

(60) Feng, R.; Peterson, K. A. Correlation consistent basis sets for actinides. II. The atoms Ac and Np–Lr. *J. Chem. Phys.* **2017**, *147*, 244106, DOI: 10.1063/1.5010587.

(61) Glendening, E. D.; Badenhoop, J. K.; Reed, A. E.; Carpenter, J. E.; Bohmann, J. A.; Morales, C. M.; Karafiloglou, P.; Landis, C. R.; Weinhold, F. NBO 6.0. 2018; Place: Madison, WI.

(62) Carter, T. J.; Wilson, R. E. Coordination Chemistry of Homoleptic Actinide(IV)–Thiocyanate Complexes. *Chem. Eur. J.* **2015**, *21*, 15575–15582, DOI: 10.1002/chem.201502770.

(63) Denning, R. G. Electronic structure and bonding in actinyl ions and their analogs. *J. Phys. Chem. A* **2007**, *111*, 4125–4143, DOI: 10.1021/jp071061n.

(64) Platts, J. A.; Baker, R. J. A computational investigation of orbital overlap versus energy degeneracy covalency in $[UE_2]^{2+}$ (E = O, S, Se, Te) complexes. *Dalton Trans.* **2020**, *49*, 1077–1088, DOI: 10.1039/C9DT04484A.

(65) Nakanishi, W.; Hayashi, S. Role of dG/dw and dV/dw in AIM Analysis: An Approach to the Nature of Weak to Strong Interactions. *J. Phys. Chem. A* **2013**, *117*, 1795–1803, DOI: 10.1021/jp3095566.

(66) Pilmé, J.; Renault, E.; Bassal, F.; Amaouch, M.; Montavon, G.; Galland, N. QTAIM analysis in the context of quasirelativistic quantum calculations. *J. Chem. Theory Comput.* **2014**, *10*, 4830–4841, DOI: 10.1021/ct500762n.

(67) Ingram, K. I. M.; Tassell, M. J.; Gaunt, A. J.; Kaltsoyannis, N. Covalency in the f Element-Chalcogen Bond. Computational Studies of $M[N(EPR_2)_2]_3$ (M = La, Ce, Pr, Pm, Eu, U, Np, Pu, Am, Cm; E = O, S, Se, Te; R = H, ^{i}Pr, Ph). *Inorg. Chem.* **2008**, *47*, 7824–7833, DOI: 10.1021/ic800835k.

(68) Wellington, J. P. W.; Kerridge, A.; Kaltsoyannis, N. Should environmental effects be included when performing QTAIM calculations on actinide systems? A comparison of QTAIM metrics for $Cs_2UO_2Cl_4$, $U(Se_2PPh_2)4$ and $Np(Se_2PPh_2)4$ in gas phase, COSMO and PEECM. *Polyhedron* **2016**, *116*, 57–63, DOI: 10.1016/j.poly.2016.02.048.